A Symmetrical Component Feature Extraction Method for Fault Detection in Induction Machines

***Abstract*—Induction motors (IMs) are among the maturest electro-mechanical technologies still in use today. Their construction and operation has greatly evolved over the course of the last century. The long automated control and continuous monitoring of IMs has benefited from modern artificial intelligence (AI) based approaches. IM automation schemes have also demonstrated the ability to provide machine fault detection and diagnosis (FDD) function. AI based FDD methods in IMs have employed frequency-domain, time-frequency, and time-domain analysis as the basis of their feature extraction schemes. A particularly promising approach is the use of symmetrical components (SCs) in time-domain FDD systems. Current SC based approaches, however, are limited in their generalizability to different fault classes, may require detailed machine models, and can suffer from computational limitations. In this proposed work, an improved feature extraction method based on SCs for a pattern recognition based FDD scheme for three-phase (3ϕ) IMs will be presented. This novel feature extraction method was implemented and verified e xperimentally. T he resultant quality and classification p erformance o f t he n ewly extracted features proved promising in increasing the generalizability and computation speed of SC-based FDD systems.**

***Index Terms*—Induction Machines, Faults, Monitoring, Fault Detection and Diagnosis, Feature Extraction, Artificial Intelligence, Machine Learning, and Symmetrical Components.**

NOMENCLATURE

α	Symmetrical component coefficient
δ	Peak prominence coefficient
$\Delta\overline{i_1}$, and $\Delta\overline{i_2}$	Derivative of average positive and negative symmetrical components
$\lambda_\alpha, \lambda_\beta$, and λ_γ	Clarke Transform components
μ_1, andμ_2	Distribution means
$\overrightarrow{I_a}, \overrightarrow{I_b}$, and $\overrightarrow{I_c}$	Sampled RMS vectors of stator currents
ψ_u, and ψ_l	Upper and Lower envelope functions
σ	Standard deviation
Σ_1, and Σ_2	Covariance matrix of distributions
$\mathrm{P_k}$	Function call for **Algorithm 1**
θ	Phase angle of measured phase a stator current
a, and A	Algorithm 1 variables
D_B	Bhattacharyya distance
h_k, b_k, c_k, and d_k	Spline function coefficients
i_0, i_1, and i_2	Samples of zero, positive, and negative symmetrical components
I_a, I_b, and I_c	RMS magnitude of measured stator current
i_a, i_b, and i_c	Samples of the measured stator current
k	Spline function index
m_k	Peak magnitude of the set k
N	Index of extracted features samples of interest
n	System sample index
N_k	Sample index for spline function of the set k
s_k	Interpolating spline function
Ts	Sample time between consecutive samples
$u[N]$	Array of extracted features: samples of interest

I. INTRODUCTION

ELECTRIC motors are a crucial component for a variety of industries, and for large quantities of commercial appliances. Today, the induction motor (IM) is the most frequently used electric motor, due to its simple construction, ease of operation, and flexibility [1, 2]. This has provoked countless electrical and mechanical design iterations [1–5]. The potential for fault conditions that cause expensive damage for both the machine and its industrial process have motivated efforts in investigating IM faults and their detection. As a result, the ability to detect and diagnose faults has become indispensable in many industrial IM application [6–11].

The detection of IM faults has greatly benefited from the progression of modern control theory [7], and now from the rapid evolution of artificial intelligence (AI) and the emergence of large volume data collection schemes [8, 12]. The trending use of AI in IM applications has led to the development of several fault detection and diagnosis (FDD) approaches, and has proven greatly beneficial for the control, operation, and human-machine interaction (HMI) of these machines [13]. The achievements of modern fault detection and identification in IMs is reviewed in reference [7], where the concept of analytical redundancy and fault-tolerant control is used. Within these concepts exists three major data processing schemes for feature extraction, including the model-based, signal-based, and knowledge-based approaches [12–15]. In practice, however, the signal-based approach using an analytical redundant controller has been noted to be the most applicable due to its ability for on-line and real-time monitoring and diagnosis of IM systems [7]. Signal-based approaches take advantage of features in either the frequency or time domains [7, 14, 16–19].

The use of the frequency-domain for feature extraction in signal-based FDDs has led to the extensive use of the discrete

Fourier transform (DFT). Popular methods include current signature analysis (MCSA) and vibration signal analysis. These methods have shown promise, but work best when the IM is in steady-state [7, 8]. In practice, however, IMs are more likely to experience dynamic and transient conditions; particularly if a variable speed drive is used. As a result, a motivation for the research and development of time-frequency methods emerged. Time-frequency analysis methods have demonstrated a remarkable ability for extracting fault features in dynamic signals with a high degree of accuracy. The references presented in the works of [7, 8, 10] describe various time-frequency methods, including the short-time Fourier transform (STFT), wavelet transform (WT), Hilbert-Huang transform (HHT), and Wigner-Ville distribution (WVD). Using these methods, the fault analysis performance for dynamic IMs is impressive, but some implementation challenges still exist. For example, these FDD methods work best with better frequency resolutions, facilitated by larger sample window sizes. This, however, comes at a cost of higher computational burden and slower speeds.

An attractive alternative to frequency and/or time-frequency signal processing is the use of time-domain methods. Time-domain FDD analysis has been noted to be accommodating when considering highly dynamic and transient signals with limited computational resources. The works by [7, 8, 10] give several examples of time-domain FDD methods, all with excellent performance. An interesting approach among these methods, however, is the use of the symmetrical component transformation to produce the feature space. Symmetrical components (SCs) offer a great deal of information about an IM's voltage or current balance, magnitude, and sequence; all useful characteristics in fault detection. The works presented in [20–25] all take advantage of SC characteristics in their proposed FDD schemes, and share some common limitations. For example, the methods presented in [20, 22, 24, 25] require detailed machine models, which distances these methods from the preferred signal-based approach. Furthermore, the methods in [20, 23] still require the computation and use of the Fourier transform and its previously noted limitations in real-time embedded applications. Lastly, all of the above methods are restricted to the detection of specific fault types (e.g. uniquely stator faults or uniquely rotor faults).

Although challenges still exist when considering SCs as the basis of a time-domain IM FDD scheme, the performance of the prior methods was still highly promising when compared to frequency-domain, time-frequency analysis, and other time-domain approaches. As a result, this work aims to introduce a non-invasive SC-based FDD scheme for IMs that is computationally inexpensive, does not require detailed machine modeling, and is generalizable to multiple fault types. The proposed method uses stator currents as the basis of the scheme, for they are easily accessible, and contain significant information about the state of the machine due to the rotor and stator windings being inductively coupled much like a transformer [26]. As a result, rotor and stator conditions can be inferred from these. Moreover, induction motor drives generally use stator currents as the inputs for their controllers [27, 28], which can facilitate the proposed method with a simple implementation for existing IM systems and possible embedding within new drive controller. The validity of the proposed method is shown experimentally with a three-phase (3ϕ), $3-hp$ IM and conventional classifier algorithms on a low-cost microprocessor. A low-cost microprocessor platform was selected to demonstrate the low computational cost of the proposed algorithms. The detection and diagnosis results of the proposed symmetrical component feature extraction (SCFE) method show a repeatable behavior when used with conventional classifiers, where each fault class demonstrated low intra-class variability and high inter-class variability. Moreover, the SCFE method can be computed within one fundamental cycle of the IM under observation, making it suitable for real-time on-line monitoring applications.

II. Induction Motor Faults

All IMs are subject to a number of possible electrical and mechanical faults see references [9, 29]) which can occur either internally or externally to the motor. For IMs, external faults are events that occur outside the motor assembly, such as a disturbance in the supply or excessive machine torque demands, while internal faults could be stator winding failures, rotor electrical faults, or rotor mechanical faults. [30]. This work focuses on the most common IM faults. Common faults include internal stator faults, which account for approximately 38% of IM fault conditions; rotor related faults, which account for 10%; and Worn down bearing faults, which relate to approximately 40% of fault conditions. All other faults (e.g. thermal, loss-of-conductor, torque overload, etc) comprise the remaining 12% of fault conditions. [9]

This work considers the stator, rotor, loss-of-conductor, and rotor torque overload conditions. Stator faults include line-line (L-L) and line-neutral (L-N) events that are commonly caused by winding insulation deterioration [32]. Rotor faults occur during broken bar events due to machine torque pulsations, imperfections in the machine construction, and mechanical stresses [9, 33]. Loss-of-conductor faults occur when a phase or two of the supply are disconnected. Lastly the rotor torque overload condition occurs when there is an excessive torque demand by the mechanical load on the IM.

III. Methodology

As aforementioned, several methods for the achievement of AI based FDD for IMs exist. These methods all rely on signal pre-processing and a feature extraction process. These steps must take place before any classification of a fault can occur. The proposed SCFE scheme is uniquely responsible for the pre-processing and feature extraction of the measured stator currents of an IM. Each step taken makes use of a digital signal processing (DSP) technique. Shown in Fig. 1 is the block diagram of the presented SCFE feature extraction process. The SCFE method only requires the stator currents of the IM, which are easily accessible and non-invasive to the

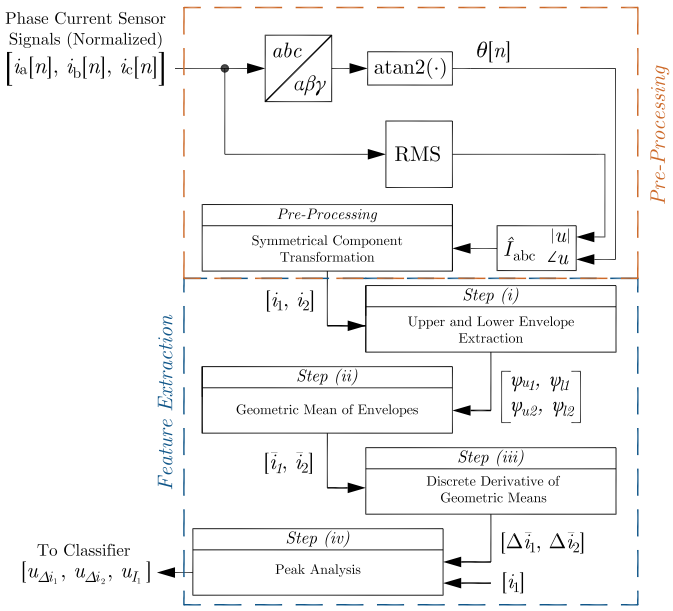

Fig. 1. Process for the proposed SCFE feature extraction method for use in IM FDD applications

machine. The following subsections will present a detailed description of each block leading to the output of the proposed SCFE scheme.

A. Input Signal Pre-Processing

The first component of the SCFE scheme is to pre-process the measured sinusoidal stator current input signals in the effort to transform them into a set of symmetrical components. Before the transformation of measured signals to SCs, additional steps are required. These steps include using the Clarke transform to acquire the signal phase, the determination of the root-mean-square (RMS) magnitude of the measured start currents, and creating a set of complex vectors to denote the stator current phasors. A mathematical description of these steps can begin with the Clarke transformation ($\alpha\beta\gamma$) such that:

$$\begin{bmatrix}\lambda_\alpha[n]\\ \lambda_\beta[n]\\ \lambda_\gamma[n]\end{bmatrix} = \begin{bmatrix}1 & -\frac{1}{2} & -\frac{1}{2}\\ 0 & \frac{\sqrt{3}}{2} & -\frac{\sqrt{3}}{2}\\ \frac{1}{\sqrt{2}} & \frac{1}{\sqrt{2}} & \frac{1}{\sqrt{2}}\end{bmatrix}\begin{bmatrix}i_a[n]\\ i_b[n]\\ i_c[n]\end{bmatrix} \tag{1}$$

where λ_α, λ_β, and λ_γ are the Clarke coefficients, and i_a, i_b, and i_c are the discrete measured stator currents. Using the Clarke coefficients the relative phase of the measured 3ϕ stator currents can be determined using the four-quadrant inverse tangent (atan2) as:

$$\theta[n] = \text{atan2}\left(\frac{\lambda_\beta[n]}{\lambda_\alpha[n]}\right) \tag{2}$$

Next, the RMS magnitude of each stator current phase is determined using a window of 512 discrete samples as:

$$I_a = \sqrt{\frac{1}{512}\sum_{n=1}^{512}(i_a[n]^2)} \tag{3}$$

$$I_b = \sqrt{\frac{1}{512}\sum_{n=1}^{512}(i_b[n]^2)} \tag{4}$$

$$I_c = \sqrt{\frac{1}{512}\sum_{n=1}^{512}(i_c[n]^2)} \tag{5}$$

The selection of a 512 point sample window for this stage was attributed to a equivalence of computational performance and solution accuracy.

Following the establishment of RMS magnitude and phase for the measured IM stator currents, a set of complex stator current vectors are defined:

$$\vec{I}_a[n] = I_a[n]e^{j\theta[n]} \tag{6}$$

$$\vec{I}_b[n] = I_b[n]e^{j\left(\theta[n]-\frac{2\pi}{3}\right)} \tag{7}$$

$$\vec{I}_c[n] = I_c[n]e^{\ j\left(\theta[n]+\frac{2\pi}{3}\right)} \tag{8}$$

Now, the SCs of the IM using the SCFE pre-processing can be determined. The SC transform is expressed as:

$$\begin{bmatrix}i_0[n]\\ i_1[n]\\ i_2[n]\end{bmatrix} = \frac{1}{3}\begin{bmatrix}1 & 1 & 1\\ 1 & \alpha & \alpha^2\\ 1 & \alpha^2 & \alpha\end{bmatrix}\begin{bmatrix}\vec{I}_a[n]\\ \vec{I}_b[n]\\ \vec{I}_c[n]\end{bmatrix} \tag{9}$$

where i_0 is the zero sequence, i_1 the positive sequence, and i_2 the negative sequence components. The variable α describes the SC phase shift coefficient and is defined as:

$$\alpha = e^{j\frac{2}{3}\pi} \tag{10}$$

Fig. 2 demonstrates examples of SCs acquired using the developed signal-preprocessing methodology for IM stator currents under various fault conditions (See *Sec. IV* for details on data acquisition). It can be observed that symmetrical faults, like rotor and mechanical failures, only produce a response in the positive sequence. This is in contrast to asymmetrical faults, such as stator short circuits, that produce a response in both the negative and positive sequence. These responses also show that symmetrical components produce a unique characteristic for each fault type, as the current response differs between fault types.

B. Feature Extraction

The second component of the SCFE method is to extract the features from the computed SCs. This final component will yield the samples to be processed by a classifier algorithm. Once more a sample window of 512 samples was selected as it offers an equilibrium between computational requirement and accuracy. The SCs are then processed through four sequential steps to yield the final output of the SCFE method; the samples

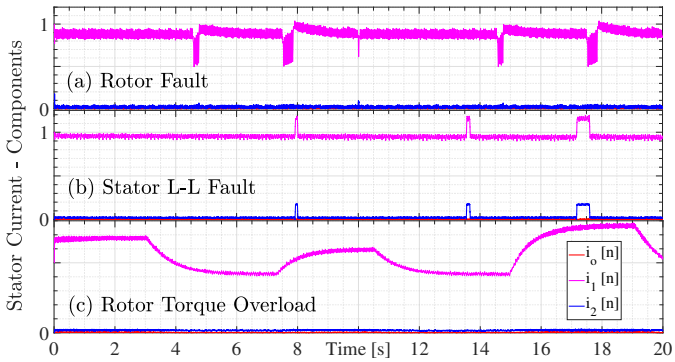

Fig. 2. Symmetrical components of IM stator currents during some common fault conditions. Faults can be observed by the disturbance in the symmetrical components.

of interest $u[N]$. The output of the SCFE produces three key repeatable and separable features, which include:

(i) the derivative of average positive SC ($\Delta\overline{i_1}$),
(ii) the derivative of average negative SC ($\Delta\overline{i_2}$),
(iii) the magnitude of the average positive SC ($|\overline{i_1}|$).

The extracted features (i) and (ii) can be obtained through processes indicated in *Steps (i) to (iii)*, while the extracted feature (iii) is obtained through *Steps (i)* and *(ii)*; before being processed in the final *Step (iv)*. A description of the *Steps (i)-(iv)* is given in the following subsections.

Step (i) - Peak Envelope

Considering the now determined discrete signals $i_1[n]$ and $i_2[n]$, the first step is determining an upper function envelope ψ_u and lower function envelope ψ_l for the positive and negative SC in the selected sample window. The envelope of the sample window is computed by considering local maxima, minima, and a spline function, s_k.

The local maxima and minima of the SCs can be determined using a procedure developed in [34]. This procedure is implemented as in the steps of **Algorithm 1**, which can detect peak values, m_k, in a signal using a finite number of samples. The finite number of samples can be represented by a sliding rectangular window of the processed signal [35]. The outputs of **Algorithm 1**, N_k and m_k, can be used with an interpolating function to calculate the upper and lower envelopes of the processed signals. In this work, the interpolating function was selected to be the cubic spline function, which can be expressed as [36]:

$$s_k[n] = m_k + b_k(n - N_k) \ldots + c_k(n - N_k)^2 + d_k(n - N_k)^3 \quad (11)$$

where

$$h_k = (N_{k+1} - N_k)T_s \quad (12)$$

$$b_k = \frac{1}{h_k}(m_{k+1} - m_k) \quad (13)$$

Algorithm 1 Algorithm for Peak Detection $f_x : \mathrm{P_k}$

Input: $A[0 \cdots 511]$, δ (Peak Prominence Coefficient)
Output: N_k, m_k

Initialization :
$n \leftarrow 1$
max $\leftarrow -\infty$; min $\leftarrow \infty$
max_index $\leftarrow 0$; min_index $\leftarrow 0$
max_flag $\leftarrow 1$

Peak Detection Loop:
while $n \leq 512$ **do**
  $a \leftarrow A[n]$

  if $a >$ max **set** max$\leftarrow a$ **and** max_index$\leftarrow n$
  if $a <$ min **set** min$\leftarrow a$ **and** min_index$\leftarrow n$

  if (max_flag **is** $true$) **and** ($a \leq$max$-\delta$) **then** {
    set $m_k \leftarrow$ max **and** $N_k \leftarrow$max_index
    set min$\leftarrow a$ **and** min_index$\leftarrow n$
    set max_flag $\leftarrow 0$ }

  else $a \geq$ min$-\delta$ {
    set max$\leftarrow a$ **and** max_index$\leftarrow n$
    set max_flag $\leftarrow 1$ }

end while

return N_k, m_k

$$c_k = 3(m_{k+1} - m_k) - 2b_k - b_{k+1} \quad (14)$$

$$d_k = 2(m_{k+1} - m_k) + b_k + b_{k+1} \quad (15)$$

The spline function, s_k, is used to determine the upper envelopes, ψ_{u_1} and ψ_{u_2}, for the positive and negative SC, that are:

$$\psi_{u_1} = s_k(\mathrm{P_k}(i_1[n])) \quad (16)$$

$$\psi_{u_2} = s_k(\mathrm{P_k}(i_2[n])) \quad (17)$$

In addition, s_k is required to calculate the lower envelopes, ψ_{l_1} and ψ_{l_2}, for the positive and negative SC. The calculation of ψ_{l_1} and ψ_{l_2} employs the inverse signals of $i_1[n]$ and $i_2[n]$ as:

$$\psi_{l_1} = s_k(\mathrm{P_k}(i_1^{-1}[n])) \quad (18)$$

$$\psi_{l_2} = s_k(\mathrm{P_k}(i_2^{-1}[n])) \quad (19)$$

Step (ii) - Geometric Mean

Following the evaluation of ψ_u and ψ_l for i_1 and i_2, the geometric mean between envelopes for the positive and negative SCs is determined. The resulting geometric mean of these envelopes is analogous to low-pass filtering (LPF) i_1 and i_2, but assures little-to-no phase shift in the output of the function, and removes any frequency dependencies in

the signals. The proposed method is uniquely concerned with the shape of the symmetrical components, not its frequency components. The geometric mean can thus be defined using ψ_l and ψ_u as:

$$\overline{i_x}[n] = \sqrt{\psi_{u_k} \times \psi_{l_k}} \quad x \in [1, 2] \tag{20}$$

The completion of this step gives the feature (iii) $|\overline{i_1}|$. This feature is directly passed to *Step (iv)* of the SCFE method. Features (i) and (ii) still require an additional processing step before being passed to *Step (iv)*.

Step (iii) - Discrete Differentiation

The discrete signals $\overline{i_1}[n]$ and $\overline{i_2}[n]$, determined in *Step iii*, give the overall shape of $i_1[n]$ and $i_2[n]$. Fault events can be further characterized differentially. As a result, changes in the current components can be greater emphasized given the sample rate. The discrete derivative can be applied as:

$$\Delta\overline{i_x}[n] = \frac{\overline{i_k}[n] - \overline{i_k}[n-1]}{T_s} \quad x \in [1, 2] \tag{21}$$

where T_s is the sampling rate of the system, which uses a regular uniform sampling scheme.

Fig. 3 demonstrates an example of the positive SC when applying the first three steps of the SCFE method for a rotor fault. From this figure, one can observe ψ_{u_1} and ψ_{l_1}; $\overline{i_1}$, and $\Delta\overline{i_1}$. (See *Sec. IV* for details on data acquisition).

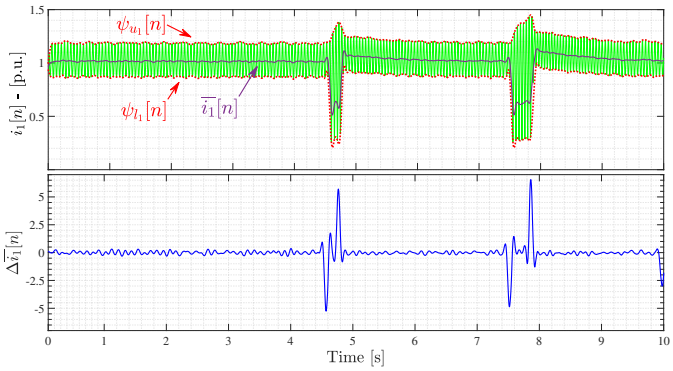

Fig. 3. Example of the proposed feature extraction method for a rotor broken bar fault. The top graph demonstrates I_1 (red), $\overline{i_1}$ (blue),ψ_u and ψ_l (dashed). The bottom graph shows the resultant $\Delta\overline{i_1}$.

C. Step (iv) - Peak Analysis (Thresholding)

Once the first three steps of the SCFE method is complete, a set of samples of interest, $u[N]$, can be determined. $u[N]$ obtains samples from the selected features using peak analysis, as denoted in **Algorithm 1**. This set of samples are selected based on a prominence value, δ, of the detected peaks. The purpose of this final step is to only allow the classification of extracted feature samples above a certain threshold that would put into question the health of the machine. The determination of $u[N]$ can be described as:

$$N \equiv \begin{cases} n \in \mathrm{P_k}(\Delta\overline{i_1}[n]) | m_k \geq \delta = 0.125 \bullet \Delta\overline{i_1}[n] \\ n \in \mathrm{P_k}(\Delta\overline{i_2}[n]) | m_k \geq \delta = 0.0125 \bullet \Delta\overline{i_2}[n] \end{cases} \quad n \in \mathbb{Z} \tag{22}$$

where N is a vector containing n samples from the evaluated peaks $\mathrm{P_k}$ in $\Delta\overline{i_1}[n]$ and $\Delta\overline{i_2}[n]$. The vector N is then be used to determine $u[N]$ such that:

$$u[N] = \left[\Delta\overline{i_1}[N], \Delta\overline{i_2}[N], |\overline{i_1}[N]|\right] \quad N \in \mathbb{Z} \tag{23}$$

Adopting thresholding in the feature extraction process reduces the number of samples passed on to an external classifier by only focusing on points of prominent fluctuation.

IV. Experimental Setup

To demonstrate the effectiveness of the SCFE method within an FDD using external classifier algorithms, data was collected from a 3ϕ wye-connected $3-hp$ wound-rotor IM coupled to a mechanical load. For this test system, the mechanical load was implemented using a DC shunt-generator terminated by a bank of power resistors. Fig. 4 shows a schematic diagram of the experimental setup including the instrumentation used in data acquisition. The stator currents of the IM motor were extracted using current transformers (CT). The CT signals were sampled using a data acquisition platform (DAQ) at a sample rate of $T_s = 400\ \mu$s.

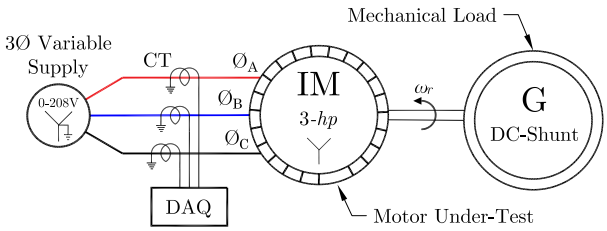

Fig. 4. Schematic diagram of the experimental system used in acquiring IM fault data.

Fig. 5 shows the laboratory implementation of the experimental setup based on the schematic diagram (see Fig. 4).

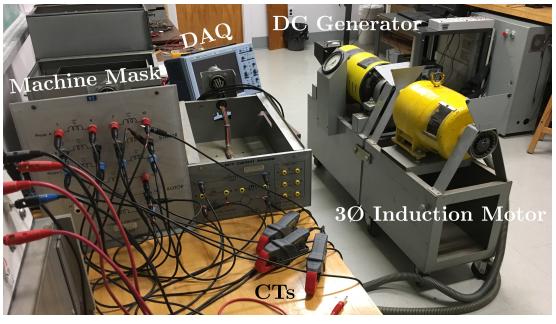

Fig. 5. Picture of the laboratory implementation of the experimental acquisition of IM fault data.

The IM used in this experiment possesses a mask that allows

access to the rotor and stator windings. As a result, electrical faults at the stator and rotor were created using using a solid-state relay between machine windings. Once operating in steady-state, the IM was subjected to momentary faults by either the opening or closing of the relay. It was noted that the rotor broken bar fault was achieved by producing an open-circuit between a few rotor windings through the machine mask. A rotor torque overload was achieved by overloading the IM through excessive power demand by the DC-generator.

An example of acquired data is shown in Fig. 6 and Fig. 7. These examples demonstrate a loss-of-conductor fault condition on the stator and a rotor broken bar fault on the IM. It should be noted that measured stator currents are scaled as a result of the CT ratios. The CTs used in this experiment were observed to have a ratio of 200mV:1A. All stator currents, once acquired, were then normalized to a per-unit (p.u.) scale. The per-unit scale for the IM under-test was based on $S_{base} = 2.2$ kVA, $V_{base} = 208$ V.

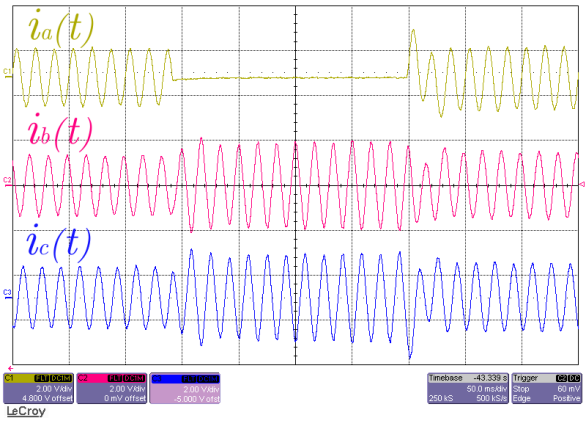

Fig. 6. Example DAQ capture for a loss-of-conductor fault condition on the stator of the IM under-test. The voltage scale is 2V/Div. and the time-base 50 ms/Div.

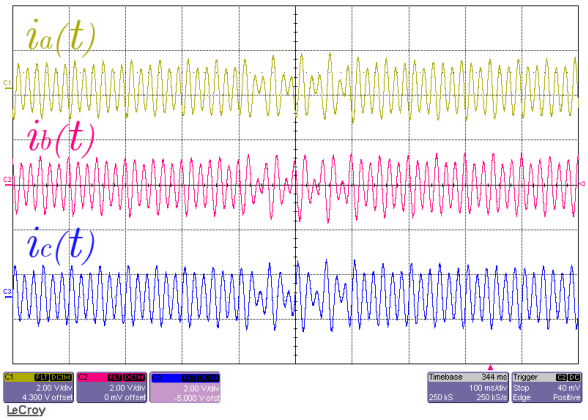

Fig. 7. Example DAQ capture for a rotor broken bar fault on the IM under-test. Stator currents are displayed. The voltage scale is 2V/Div. and the time-base 100 ms/Div.

V. Evaluation

The SCFE method was evaluated in two steps. First, the performance of the extracted features was evaluated, and second, the performance was compared using a handful of common classifiers that considered the $u[N]$ from the selected features. Both a micro-computer and desktop computer were used in the performance evaluation of the SCFE method.

A. Extracted Feature Performance

Feature extraction performance was evaluated by observing the quality of extracted features, and the time required to obtain the features given a new sample point. The overall quality of $u[N]$ obtained using SCFE method, was evaluated using two primary factors; the inter-class and intra-class variability of the fault and no-fault classes. These two aspects are fundamental to the performance of any classification system, as they characterize the overall discriminability of feature space. Desirably, each class should exhibit high inter-class variability, while maintaining low intra-class variability. Fig. 8 demonstrates these important aspects for the extracted $u[N]$. One can observe that the normal and fault $u[N]$ exhibit these desired behaviors for each data class.

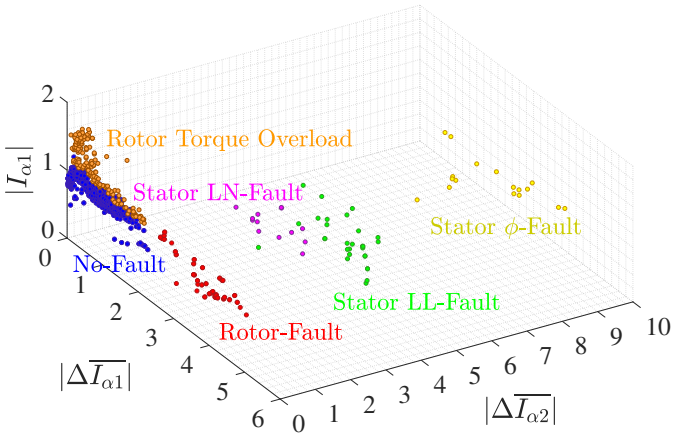

Fig. 8. A 3-Dimensional scatter plot demonstrating $u[N]$ yielded from the extracted features set. The classes for each collection of data points are labeled.

In addition, the Bhattacharyya distance, D_B, was evaluated between data classes. This distance metric was used to further support the observed inter-class variance of $u[N]$. For multivariate distributions, D_B is described as [32]:

$$D_B = \frac{1}{8}(\mu_2 - \mu_1)^T \left[\frac{\Sigma_1 + \Sigma_2}{2}\right]^{-1} (\mu_2 - \mu_1)... + \frac{1}{2}\ln\left(\frac{\left|\frac{\Sigma_1+\Sigma_2}{2}\right|}{\sqrt{|\Sigma_1||\Sigma_2|}}\right) \quad (24)$$

Where μ is the mean of the distribution and Σ is the covariance matrix. The results from D_B, Table I, reflect the distance between two data cluster μ in terms of standard deviations σ.

It can be noted that a majority of the data classes have a $D_B > 3\sigma$, meaning very little confusion exists between these fault distributions. It was found that $D_B < 2\sigma$ between L-L and L-N fault classes, as well as between the normal operating condition and rotor torque overload fault. This signifies that

TABLE I
BHATTACHARYYA DISTANCE BETWEEN FAULT CLASSES

	No-Fault	**Mech.**	**L-L**	**L-N**	**Open-ϕ**	**Rotor**
No-Fault		1.517	29.082	14.891	30.671	4.097
Mech.	1.517		27.752	15.362	29.380	3.594
L-L	29.081	27.751		1.853	12.570	16.974
L-N	14.891	15.361	1.853		15.642	12.336
Open-ϕ	30.670	29.380	12.570	15.642		32.783
Rotor	4.097	3.593	16.974	12.336	32.783	

some confusion exists between these distribution pairs. Even-though these distributions overlap, $D_B > 1.5\sigma$ which suggests that only approximately 10% of data points overlap between classes.

Next, the time required to obtain and compute $u[N]$ was evaluated. The evaluation was carried out on an Espressif ESP32: an embedded dual-core 32-bit micro-computer operating at a clock speed of 160 MHz. A micro-computer was selected as the platform of choice for this test as it reflects a practical embedded implementation of the SCFE method. This evaluation took into consideration the time from when a new sample is acquired until it is used by the classifier. It was found that on average, the SCFE method produced $u[N]$ within 7.4 ms of receiving a new sample. This corresponds to approximately half of a IM current cycle. Fig. 9 shows a breakdown of processing time for each step of the SCFE method on a single core of the micro-computer.

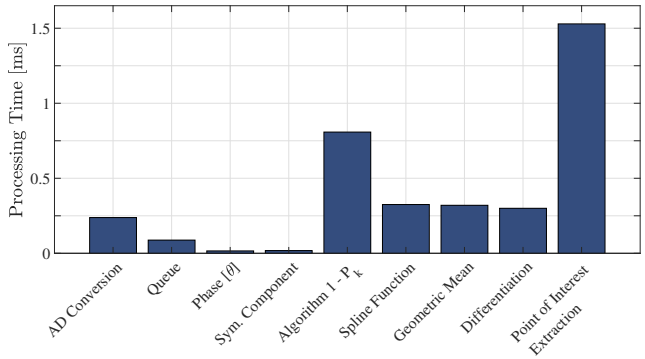

Fig. 9. Processing time for each discrete step of the SCFE method.

B. Classifier Performance

Multiple classifiers were investigated to evaluate the robustness of the new features to different classifiers, and to determine which classification scheme would yield the fastest and most accurate results using data from the SCFE method. The following classifiers were evaluated:

(i) Linear Discriminant Classifier (LDA)
(ii) Quadratic Discriminant Classifier (QDA)
(iii) Naïve Bayes Classifier (NB)
(iv) CART Decision Tree Classifier (CART)
(v) k-Nearest Neighbor Classifier (KNN)
(vi) Support Vector Machine Classifier (SVM)
(vii) Ensemble Decision Tree Classifier (ENS)

These classifiers were implemented in a MATLAB environment, which was installed on a standard workstation computer (4.0 GHz Quad Core Processor, 8 GB Memory, Disk Drive). The classifiers made use of only a single thread on the central processing unit (CPU) to avoid introducing timing complexity due to computational concurrency. Each classifier's parameters were optimized with MATLAB's built-in functionality in order to maximize its prediction accuracy. The data used to train the classifiers were taken from random time positions during the associated fault conditions. These data samples were processed to extract the features mentioned previously. The classifiers were then trained with over 400 feature samples from all six fault classes.

The prediction times were evaluated for each of the selected classifiers using the extracted data-set. It was noted that all the tested classifiers produced results in less than 1.5 stator current cycles in producing accurate performance results. Fig. 10 shows classifier prediction times. It can be seen from

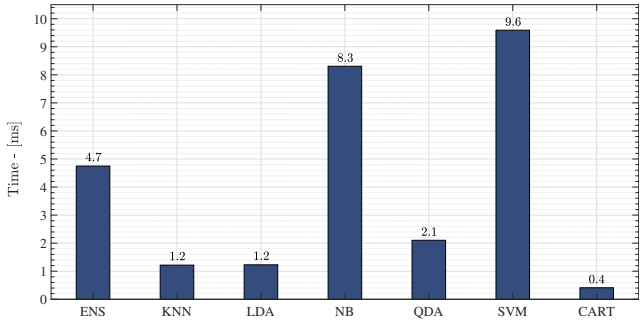

Fig. 10. A bar chart showing the time taken for each classifier to predict the class of one data point

Fig. 10 that the CART decision tree produced the lowest prediction times of all classifiers. This result is due to the CART classifier using logical statements over mathematical and/or statistical models to determine the class of a new data point. Next, the KNN and LDA algorithms were the second fastest algorithms, immediately followed by the QDA classifier. Both the LDA and QDA are parametric classifiers that simplify data models through statistical assumptions, and as a result faster classification can be achieved. Unlike LDA and QDA, the KNN is a non-parametric classifier, but benefits from the simplicity of its algorithm. It should be noted that KNN classifiers slow down with the addition of more training data. The ENS, NB, and SVM classifiers were found to be the slowest algorithms.

To evaluate the classification performance of the system, the mean error and inter-class error were evaluated using ten-fold cross-validation of the full data-set. Fig. 11 shows the mean error of each classifier, where the error of each class was equally weighted in the determination of the classifier mean error. It can be observed that all classifiers produced average errors below 2%. Comparing Fig. 10 and Fig. 11, it can be seen that classifier accuracy ranking is roughly the opposite of computation time ranking. The CART decision

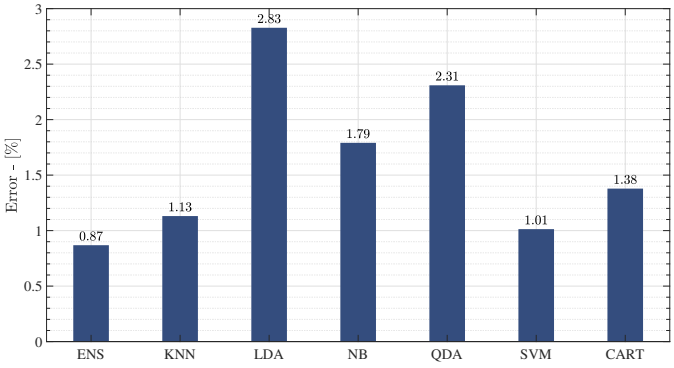

Fig. 11. The errors of each classifier given a 10-fold cross validation of the sample data

tree, however, was the fastest classification algorithm and produced results comparable to the most accurate classifiers. Fig. 12 shows additional detail about the class specific errors for each classifier. As predicted by the D_B analysis, it can

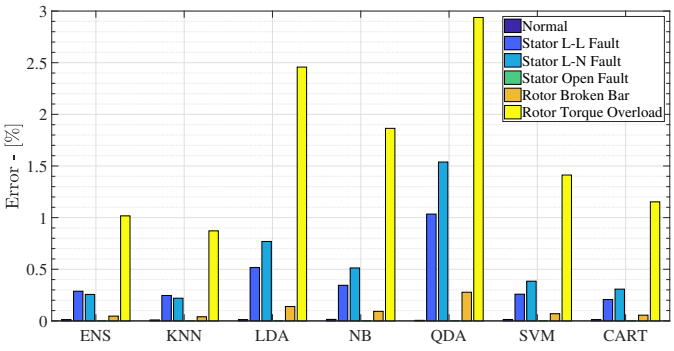

Fig. 12. The error rate of each fault type organized by classifier

be observed that the rotor torque overload class had higher errors than any other class for all classifiers. The inclusion of additional features focused on separating normal and rotor torque fault could prove beneficial in the reduction of this error.

VI. Conclusions

In this work, a novel feature extraction method was proposed and evaluated on 3ϕ $3-hp$ IM under various common fault conditions. The proposed SCFE method showed an ability to offer rapid and accurate computation when analyzing and extracting features from measured time-domain stator current SCs through the use of an embedded micro-computer. The unique use of stator currents as the input of the SCFE also supports possible implementation and embedding of the SCFE in IM drive controllers. The extracted features by the SCFE exhibited low intra-class variability and high inter-class variability. These extracted feature characteristics were further supported by the performance of a number of well-known classifier algorithms, which were provided with the output of the SCFE method. Experimental test demonstrated that well-known classifiers were able to provide classification error as lows as 0.87%, and produce a result in less than 0.7 fundamental IM cycles, or 11.7 ms when using the features extracted by the proposed SCFE. Moreover, the greater generalizability between multiple fault classes of the proposed SCFE method suggests real promise for IM FDD applications. For the detection of a greater number of fault types by one scheme may reduce the duration a fault is sustained on an IM, and potentially help in the early intervention using an appropriate fault mitigation.

VII. Future Work

The promising performance of the proposed SCFE method has demonstrated its feasibility for potential IM applications. Future developments of the SCFE could include a full and embedded integration with a classification algorithm such as the CART decision tree in a digital IM protection scheme. To further the generalizability of the SCFE scheme, additional features could be investigated for other faults such as: core faults, bearing failures, air gap eccentricity conditions, and thermal failures. There is also potential for the extension of this scheme to other electric machine types, such as synchronous machines.

References

[1] I. Boldea and S. A. Nasar, "Induction Machines: An Introduction," in *The Induction Machine Handbook*, Boca Raton, FL: CRC Press, 2002, pp. 13

[2] E. R. Laithwaite, "The Way Ahead," in *IEEE Transactions on Magnetics*, vol. 27, no. 1, pp. 7-10, Jan. 1991

[3] M. Poloujadoff, "Linear Induction Machines: I. History and Theory of Operation," in *IEEE Spectrum*, pp. 72-80, Feb. 1971

[4] E. R. Laithwaite, "Linear Electric Machines - A Personal View," in *Proceedings of the IEEE*, vol. 63, no. 2, pp. 250-315, Feb. 1975

[5] D. F. Alaxander, "Recent Improvements in Large Induction Motors," in *Journal of the A.I.E.E.*, vol. 46, no. 11, pp. 1167-1175, Nov. 1927.

[6] A. Siddique, G. S. Yadava, and B. Singh, "A Review of Stator Fault Monitoring Techniques of Induction Motors," in *IEEE Transactions on Energy Conversion*, vol. 20, no. 1, pp. 106-115, March 2005

[7] Z. Gao, C. Cecati, and S. Ding, "A survey of Fault Diagnosis and Fault-Tolerant Techniques Part I: Fault Diagnosis with Model-Based and Signal-Based Approaches," in IEEE Transactions on Industrial Electronics, vol. 62. No. 6, pp. 3757-3767, June 2015.

[8] A. Bellini, *et a.l.*, "Advances in Diagnostic Techniques for Induction Machines", in *IEEE Transactions on Industrial Electronics*, vol. 55, no. 12, pp. 4109-4126, December 2008.

[9] W. T. Thomson, and M. Fenger, "Current Signature Analysis to Detect Induction Motor Faults," in *IEEE Industrial Applications Magazine,* vol. 7, no. 4, pp.26-34, July/August 2001.

[10] H. Henao, *et all*, "Trends in Fault Diagnosis for Electrical Machines: A Review of Diagnosis Techniques", in *IEEE Industrial Electronics Magazine,* vol. 8, no. 2, pp. 31-42, June 2014

[11] F. Filippetti, G. Franceschini, C. Tassoni, and P. Vas, "Recent Developments of Induction Motor Drives Fault Diagnosis Using Techniques," in *IEEE Transactions on Industrial Electronics,* vol. 46, no. 5, October 2000.

[12] A. Giantomassi F. Ferracuti S. Iarlori, G. Ippoliti, and S. Longhi, "Electric Motor Fault Detection and Diagnosis by Kernel Density Estimation and KullbackLeibler Divergence Based on Stator Current Measurements," in *IEEE Transactions on Industrial Electronics,* vol. 62, no. 3, pp. 1770-1781, Mar. 2015

[13] R. Vepa, "A Review of Techniques for Machine Learning of Real-Time Control Strategies," in *Intelligent Systems Engineering,* vol. 2, no. 2, pp. 77-90, Summer 1993

[14] T. Ince, S. Kiranyaz, L. Eren, M. Askar, and M. Gabbouj, "Real-Time Motor Fault Detection by 1-D Convolutional Neural Networks," in *IEEE Transactions on Industrial Electronics,* vol. 63, no. 11, pp. 7067-7076, Nov. 2016.

[15] I. Martin-Diaz, D. Morinigo-Sotelo, O. Duque-Perez, and R. J. Romero-Troncoso, " Early Fault Detection in Induction Motors Using AdaBoost With Imbalanced Small Data and Optimized Sampling," in *IEEE Transactions on Industry Applications,* vol. 53, no. 3, pp. 3066-3076, May 2017.

[16] I. González-Prieto, M. J. Duran, N. Rio-Garcia, F. Barrero, and C, Martí, "Open-Switch Fault Detection in Five-Phase Induction Motor Drives Using Model Predictive Control," in *IEEE Transactions on Industrial Electronics,* vol. 65, no. 4, pp. 3045-3056, Jan. 2017.

[17] M. Irhoumah, R. Pusca, E. Lefevre, D. Mercier, R. Romary, and C. Demian, "Information Fusion With Belief Functions for Detection of Inter-turn Short-Circuit Faults in Electrical Machines Using External Flux Sensors," in *IEEE Transactions on Industrial Electronics,* vol. 65, no. 3, pp. 2642-2653, Mar. 2018.

[18] S. E. Pandarakone, Y. Mizuno, and H. Nakamura, "Distinct Fault Analysis of Induction Motor Bearing Using Frequency Spectrum Determination and Support Vector Machine," in *IEEE Transactions on Industry Applications,* vol. 53, no. 3, May 2017

[19] S. Wu, and T. W.S. Chow, "Induction Machine Fault Detection Using SOM-Based RBF Neural Networks," in *IEEE Transactions on Industrial Electronics,* vol. 51, no. 1, pp. 183-195, Feb. 2004

[20] M. B. K. Bouzid, and G. Champenois, "New Expressions of Symmetrical Components of the Induction Motor Under Stator Faults," in *IEEE Transactions on Industrial Electronics,* vol. 60, no. 9, pp. 4093-4102, September 2013.

[21] M. Arkan, D. K. Perovic, and P. Unsworth, "Online stator fault diagnosis in induction motors," in *Proceedings of the IEE,* vol. 148, no. 6, pp. 537-547, November 2001.

[22] D. G. Dorrell, and K. Makhoba, "Detection of Inter-Turn Stator Faults in Induction Motors Using Short-Term Averaging of Forward and Backward Rotating Stator Current Phasors for Fast Prognostics," in *IEEE Transactions on Magnetics,* vol. 53, no. 11, pp. 1-7, November 2017.

[23] D. G. Jerkan, D. D. Reljic, and D. P Marcetic, "Broken Rotor Bar Fault Detection of IM Based on the Counter-Current Braking Method," in *IEEE Transactions on Energy Conversion,* vol. 32, no. 4, pp. 1359-1366, December 2017.

[24] J. Yun, K. Lee, K.-W. Lee, S. Lee, and J.-Y. Yoo,"Detection and Classification of Stator Turn Faults and High-Resistance Electrical Connections for Induction Machines," in *IEEE Transactions on Industry Applications,* vol. 45, no. 2, March/April 2009.

[25] S. B. Lee, M. Tallam, T. G. Habetler, "A Robust, On-Line Turn-Fault Detection Technique for Induction Machines Based on Monitoring the Sequence Component Impedance Matrix," in *IEEE Transactions on Power Electronics,* vol. 18, no. 3, pp. 865-872, May 2003.

[26] R. Rankin, "The Induction Motor.," in *Journal of the Institution of Electrical Engineers,* vol. 39, no. 186, pp. 714-728, September 1907.

[27] M. P. Kazmierkowski, L. G. Franquelo, J. R. Marcelo, A. Perez, and J. I. Leon "High-Performance Motor Drives," in *IEEE Industrial Electronics Magazine,* vol. 5, no. 3, pp. 6-26, September 2011.

[28] E. Levi, R. Bojoi, F. Profumo, H.A. Toliyat, and S. Williamson, "Multiphase induction motor drives a technology status review," in *IET Electr. Power Appl.,* vol. 1, no. 4, pp. 489-516, July 2007.

[29] M. A. Awadallah, and M. M. Morcos, "Application of AI Tools in Fault Diagnosis of Electrical Machines and Drives An Overview," in *IEEE Transactions on Energy Conversion,* vol. 18, no.2, pp. 245-252, June 2003.

[30] R. Maier, "Protection of Squirrel-Cage Induction Motor Utilizing Instantaneous Power and Phase Information ," in *IEEE Transactions on Industry Applications,* vol. 28, no. 2, pp. 376-381, March/April 1992.

[31] A. Bellini, F. Filippetti, C. Tassoni, and G. Capolino, "Advances in Diagnostic Techniques for Induction Machines," in *IEEE Transactions on Industrial Electronics,* vol. 55, no. 12, pp. 4109-4127, Dec. 2008.

[32] L. O. Jimenez, and D. A. Landgrebe, "Supervised Classification in High-Dimensional Space: Geometrical, Statistical, and Asymptotical Properties of Multivariate Data," in *IEEE Transactions on Systems, Man, and Cybernetics-Part C: Applications and Reviews,* vol. 28, no. 1, pp. 39-55, Feb. 1998.

[33] S. Nandi, "Detection of Stator Faults in Induction Machines Using Residual Saturation Harmonics," in *IEEE Transactions on Industry Applications,* vol. 42, no. 5, pp. 1201-1209, Sept./Oct. 2006.

[34] E. Billauer, "peakdet: Peak detection using MATLAB", 2012. [Online]. Available: http://http://billauer.co.il/peakdet.html. [Accessed: 4- April-2018].

[35] M. Wolkiewicz, G. Tarchaa, T. Orowska-Kowalska and C. T. Kowalski, "Online Stator Interturn Short Circuits Monitoring in the DFOC Induction-Motor Drive," in *IEEE Transactions on Industrial Electronics,* vol. 63, no. 4, pp. 2517-2528, April 2016.

[36] S. C. Chapra, "Cubic Splines," in *Applied Numerical Methods with MATLAB for Engineers and Scientists,* ed. 3, chap. 18, New-York: McGraw Hill, 2012, pp. 438-441.

2019-09

A symmetrical component feature extraction method for fault detection in induction machines

St-Onge, Xavier F.

IEEE

https://doi.org/10.1109/TIE.2018.2875644